IOP PUBLISHING MEASUREMENT SCIENCE AND TECHNOLOGY
Meas. Sci. Technol. **19** (2008) 000000 (13pp) UNCORRECTED PROOF

Direct calibration framework of triple-hole pressure probes for incompressible flow

K M Argüelles Díaz, J M Fernández Oro and E Blanco Marigorta

Fluid Mechanics Group, University of Oviedo, Campus de Viesques, 33271, Gijón (Asturias), Spain

E-mail: arguelleskatia@uniovi.es

Received 19 December 2007, in final form 23 April 2008
Published DD MMM 2008
Online at stacks.iop.org/MST/19/000000

Abstract

This paper carries out a mathematical analysis of the limits and data reduction techniques of three-hole pressure (THP) probes operating in a 'non-nulling' mode for incompressible flow. As a result of this analysis, a direct procedure is advanced, based on the distinction of several zones within the angular range, where different relations can be applied to obtain the flow variables. This proposal provides a considerable increment of the operative angular range of THP probes: about $\pm 70^\circ$ instead of the typical $\pm 35^\circ$ for a cylindrical probe. This may extend the application of these probes in highly unsteady flows, or reduce the acquisition and data reduction effort minimizing the necessity of probe reorientation. The influence of the data reduction technique on the uncertainty transmission is also presented in the paper. From detailed considerations, it is demonstrated that the results uncertainty depends on the specific probe, but it is unaffected by the mathematical procedure employed to calculate the flow variables. Validation measurements with pneumatic probes have been made for Reynolds numbers from 4×10^3 to 3.5×10^4. In addition, a highly unsteady measurement in a low-speed axial flow fan is succinctly analysed. Taking into account both attainable angular range and uncertainty, it is determined that the optimal construction angle for the holes of a low frequency response THP probe lies between 30° and 60°, while for fast response probes, in order to avoid the separated flow region, the optimal construction angle is around 30°.

Keywords: three-hole pressure probe, flow measurement, calibration

Nomenclature

BPF	Blade passing frequency
DHW	Dual hot wire
LHS	Left-hand side
THP	Three-hole probe
α_i	Generic coefficient, numerator
b_i	Generic coefficient, denominator
C_α	Angular coefficient
C_p	Pressure coefficient
C_{Po}	Total pressure coefficient
C_{Ps}	Static pressure coefficient
f_i	Pressure coefficient
F	Function of the angle α
I_α	Angle uncertainty ($^\circ$)
I_P	Pressure uncertainty (Pa)
I_{Pd}	Dynamic pressure uncertainty (Pa)
I_{Ps}	Static pressure uncertainty (Pa)
P_i	Pressure measurement (Pa)
P_d	Dynamic pressure (Pa)
P_0	Total pressure (Pa)
P_s	Static pressure (Pa)
Re	Reynolds number
t	Time (s)
T_R	Rotor blade passing period (s)
v	Flow velocity (m s^{-1})

Greek letters

α	Flow angle (yaw angle) ($^\circ$)
α_m	Flow angle error ($^\circ$)
δ	Construction angle of the probe ($^\circ$)

λ Generic parameter
σ Standard deviation

Subscripts

i $i = 1, 2, 3$

Superscripts

$'$ Derivative
$*$ Particular measurement
$**$ Particular measurement

1. Introduction

The derivation of the flow velocity from pressure measurements requires special probes (Pitot-static probes, multi-hole probes, NACA pressure probes...) and data reduction techniques based on nonlinear mathematical relations. The capacities and limits of the measuring system (in terms of operative ranges and accuracy) depend not only on the sensors performance, but also on the probe characteristics, including associated fluid dynamic phenomena (desirable or not). For instance, in the case of a typical Pitot-static probe, it is possible to measure accurately the velocity magnitude only if the probe is aligned with the flow [1].

On the other hand, important limitations of the measuring system usually come from the mathematical relations employed to link measured and transformed variables, and also from the procedure used to calculate such relations. A classical example of this problem is observed when using THP probes to measure both direction and velocity magnitude of two-dimensional flows. The mathematical indetermination that arises in the calculation of the flow angle—at $+37^\circ$ and -37° for cylindrical THP probes—leads to consider that the maximum angular range of the probe is about $\pm 35^\circ$ [2]. It would be useful to increase these span because particular flows, mainly in turbomachinery, have instantaneous velocities with angular variations beyond that range [3]. Furthermore, although the angular span is usually enough to cover the angular oscillations, changes in the direction of the mean flow between different measuring positions require to modify the probe orientation. This procedure is time consuming because several tries are necessary in each position to centre the angular range (together with the data reduction) for the adequacy of the results.

This paper analyses the physical phenomena susceptible to condition the performance of THP probes, explaining the reasons that produce indeterminations in the mathematical calculation of the flow angle. As a consequence, it will be possible to determine the real physical range of the probes, as well as the mathematical procedures that can be employed to exploit the whole angular range.

Pressure probes with multiple holes are typically used to measure the pressure and the velocity in the case of incompressible flow. Three-hole probes obtain the direction and the velocity magnitude in a plane, whereas other probes with four, five and seven holes are able to describe three-dimensional flows. References [4, 5] provide a complete review of the different geometries used in multi-hole pressure probes, including its characteristics and basic performance. Applications of this type of probes are described in [6–9].

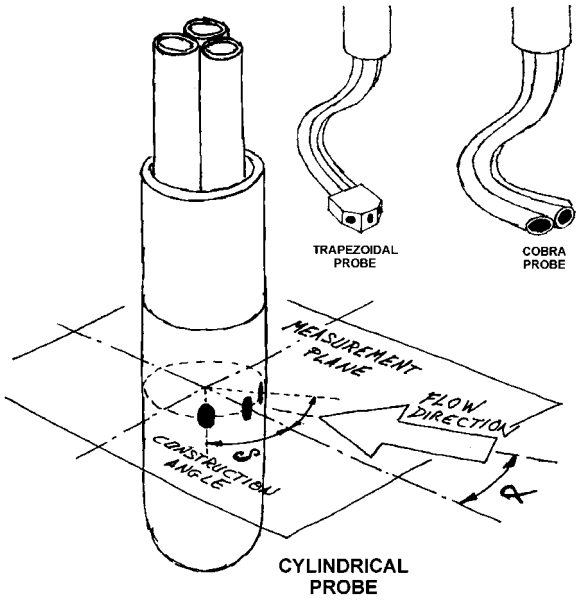

Figure 1. Three-hole pressure probes: cylindrical, trapezoidal and cobra-type geometries.

Pressure probes provide both the pressure and the velocity of the flow field. This is a major advantage when compared to anemometric techniques or laser-doppler velocimetry. In addition, pressure probes are more robust than hot-wire probes and easier to operate than optical anemometers. Furthermore, it is possible to build miniature pressure probes with high-frequency response [10], enabling us to measure unsteady flows [11] and even turbulence [12]. Reference [13] summarizes the basic characteristics of these three measuring techniques.

Figure 1 shows a sketch of a cylindrical, a trapezoidal and a cobra-type three-hole probe, detailing the reference angles in the measurement plane. The flow angle, denoted as α, is the angle between the incidence of the flow and the front axis of the probe, whereas the construction angle, denoted as δ, is the angle between the central and the lateral holes. In the case of cylindrical probes, the pressure variations in the holes with the flow angle are smooth, and very similar to the pressure distribution around a two-dimensional cylinder. In contrast, trapezoidal and cobra-type probes present abrupt edges where the flow can be easily detached.

Multi-hole pressure probes can be operated in two different ways, usually known as 'nulling' and 'non-nulling' modes. In 2D incompressible flow, both modes require pressure measurements in three different holes. When operating in the 'nulling' mode, the probe is rotated to balance the pressure in the lateral holes. The probe is thus aligned with the flow direction and the central hole measures the stagnation pressure [14]. In terms of data processing, it is the simplest operating mode of the probe, but it takes a long time to align the probe in each measurement point. In practice, this means that only steady flows can be measured using

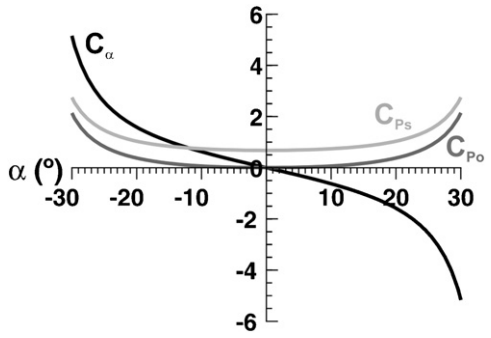

Figure 2. Angular distribution of traditional calibration coefficients.

this mode. In the 'non-nulling' mode, the probe position is fixed and the flow angle is determined from the pressure differences between the lateral holes. These pressure values are correlated with the velocity magnitude and direction of the flow through a previous calibration [15]. The 'traditional' normalized calibration coefficients used with three-hole probes are [16]

$$C_\alpha = \frac{P_2 - P_3}{P_1 - 0.5(P_2 + P_3)}$$
$$C_{P_0} = \frac{P_0 - P_1}{P_1 - 0.5(P_2 + P_3)} \qquad (1)$$
$$C_{P_s} = \frac{P_0 - P_s}{P_1 - 0.5(P_2 + P_3)}$$

where C_α represents the angular coefficient, and C_{Po} and C_{Ps} are the total and static pressure coefficients. P_o and P_s are the total and static pressure, whereas P_1, P_2 and P_3 represent the pressures measured in the central, left and right holes, respectively.

In a typical calibration procedure, the probe is placed inside a uniform flow of known characteristics. Its angular position is progressively changed over the desired range. For each position, the pressure in the probe holes, the angle and the velocity and static pressure of the flow are stored. Afterwards, the calibration coefficients defined in (1) are obtained. Figure 2 shows a typical angular distribution of those coefficients, i.e., the variation of C_α, C_{Po} and C_{Ps} with the flow angle α. Later on, the data reduction procedure employs those curves to calculate the direction and velocity magnitude of the measured flows. When the probe is used to measure an unknown flow, the pressures in the three holes are recorded, and the value of C_α for each measurement is obtained using the first expression in (1). From the C_α calibration curve, the flow angle α is determined. Once α is known, the values of C_{Po} and C_{Ps} for that particular angle are obtained from their own calibration curves. Then, P_o and P_s are calculated with the second and third expressions in (1). Finally, the difference between them, i.e. the dynamic pressure, provides the velocity magnitude of the flow.

Some authors have attempted to derive mathematical fittings for the curves of the calibration coefficients, so discrete numerical methods should not be necessary to obtain the flow variables [17, 18]. However, it is more accurate to employ the calibration coefficients directly determined from the measurements in the calibration sequence, and then obtain the flow variables with a numerical interpolation of the coefficients. The errors magnitude with this methodology is significantly lower than in the case of any mathematical fitting. Typically, this methodology when applied to the experimental calibration coefficients is known as 'direct calibration' of a pressure probe [19].

The operative angular range of a pressure probe depends on its own characteristics (number of holes, angle between them, head geometry . . .) and also of the data reduction procedure used to obtain the flow variables. When a traditional calibration is employed, typical attainable ranges are $\pm 35^\circ$ for three-hole probes [2], $\pm 25^\circ$ for five-hole probes [20] and $\pm 70^\circ$ and even $\pm 80^\circ$ for seven-hole probes [21, 22]. In this case, the factors limiting the angular range are related to the presence of singular and double points in the calibration coefficients. It will be shown that this constraint is more restrictive than the physical limit associated to fully-detached conditions in several holes of the probe. The most typical construction angles are 30° and 45°, but probes with other angles are not unusual. This angle affects the sensitivity (uncertainty) of the results but also the maximum range and the angle where singularities arise.

In this paper, a theoretical analysis of the direct calibration and data reduction procedure of a three-hole pressure probe is developed. The objective is the definition of a methodology to increase the attainable angular range of THP probes, maintaining the uncertainty of the results in acceptable levels. Following sections contain a deep mathematical analysis of the pressure distribution equations in the holes of a THP probe. In particular, the conditions leading to the existence of singular points in the data reduction equations are analysed in detail. Moreover, a new methodology for data reduction is proposed to prevent its influence on the operative angular range. In addition, the conditions inducing the appearance of double points are also studied extensively. The influence of the angular distance between the holes is also included in the discussion, in order to establish the adequate interval for the construction angle in a THP probe.

2. Mathematical analysis

From a mathematical perspective, in the equation relating the flow angle with the pressure values measured in the probe holes, two different factors may impose severe limitations. First of all, the function must be defined over the whole range, i.e., there cannot be singular points through the equation. Secondly, the flow angle must be determined univocally, that is, the equation should not present double solutions (double points). In fact, the singular points are not a real problem because they can be avoided defining different zones inside the angular range and applying different equations for every segment. In contrast, double points could be a serious problem because of their characteristic physical nature. However, the maximum physical angular range is broader than usually assumed. This section demonstrates that with an adequate election of the number of zones and its associated equations, the angular range for a typical cylindrical probe can be improved to $\pm 70^\circ$.

2.1. Determination of the flow angle

The traditional angular coefficient is only a particular method to solve a set of equations. Such a coefficient is just a relation between the pressures measured in the probe holes, depending exclusively on the flow angle. Hence, it is neither influenced by the velocity magnitude nor by the static pressure.

The pressure distribution in a probe hole can be expressed as a relation between the static pressure P_s, the dynamic pressure P_d and a particular function of the flow angle $f(\alpha)$. Therefore, the pressure distributions in the holes of a THP probe constitute a three-equation system:

$$\begin{cases} P_1 = P_s + P_d f_1(\alpha) \\ P_2 = P_s + P_d f_2(\alpha) \\ P_3 = P_s + P_d f_3(\alpha) \end{cases} \quad (2)$$

where P_1, P_2 and P_3 are the pressures measured in the holes (known variables), and P_s, P_d and α are the unknown variables corresponding to the flow to be determined. The functions $f_1(\alpha)$, $f_2(\alpha)$ and $f_3(\alpha)$ are the pressure coefficients in each probe hole. They are usually obtained from the calibration of the probe, as a discrete function of the flow angle. Theoretically, in the case of a cylindrical probe with an angular distance δ between the holes, the function $f_1(\alpha)$ is the pressure coefficient over a 2D cylinder $C_p(\alpha)$, whereas functions $f_2(\alpha)$ and $f_3(\alpha)$ are the same pressure coefficient shifted δ°—$C_p(\alpha + \delta)$ and $C_p(\alpha - \delta)$, respectively. However, it was preferred to consider them as different functions, so the analysis is not restricted to cylindrical probes. Moreover, it is thus possible to implicitly include particular manufacturing imperfections of the probes (misalignments, slight differences of the construction angle, . . .).

The flow angle cannot be explicitly derived from the three-equation system (2) because the pressure coefficients $f_i(\alpha)$ are not a direct analytical expression. They are only known in a discrete form from the calibration of the probe. In contrast, both static and dynamic pressures can be expressed in an explicit form from the equation system. The simplest mathematical solution for (2) consists in reducing the three equations into a single expression depending exclusively on the flow angle α. For instance, subtracting the first equation from the second one, the second from the third one, and then dividing both subtractions, it yields

$$\frac{P_1 - P_2}{P_2 - P_3} = \frac{f_1(\alpha) - f_2(\alpha)}{f_2(\alpha) - f_3(\alpha)} \equiv F(\alpha) \quad (3)$$

which is a function only of the flow angle. The angle cannot be obtained analytically from expression (3), but as the function $F(\alpha)$ is known from the calibration of the probe, it is possible to employ a discrete numerical method to determine α.

2.2. Singular points

Equation (3) degenerates in a singular point when the denominator is zero. For example, assuming that P_2 and P_3 are the pressure in the left and right holes respectively, the function $F(\alpha)$ is undefined at $\alpha = 0^\circ$ when both pressures are equal. The traditional calibration solves the equation system using an alternative relation—first equation in (1)—where the denominator is $P_1 - 0.5(P_2 + P_3)$. This way, the singularity is symmetrically displaced from the central point. The angles where the coefficient is now undefined depend on the probe characteristics; for a typical cylindrical probe they appear at -37° and $+37^\circ$ approximately. As a consequence, this has led to consider that the angular range is $\pm 35^\circ$. Some authors have proposed to avoid this singularity using the real dynamic pressure P_d as the denominator. The velocity is not known *a priori*, but a simple iterative procedure is employed to found the correct value [23]. Apparently this solves the singularity in the angular coefficient, but in fact the same mathematical problem arises now in the correction equation.

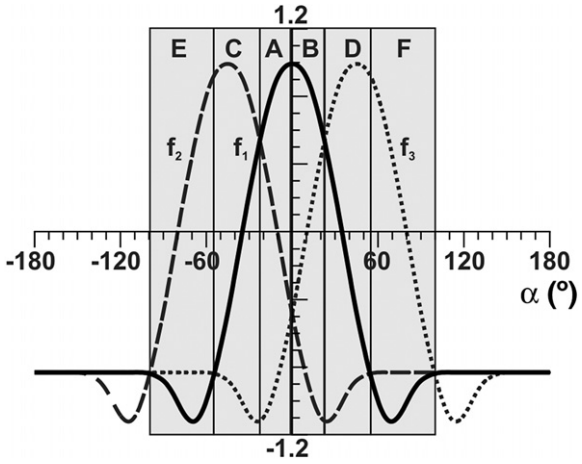

Figure 3. Possible zones dividing the angular range for a cylindrical probe with $\delta = 45^\circ$.

However, the singularities can be avoided discriminating several zones in the whole angular range, and defining an adequate relation $F(\alpha)$ in each one of them. Actually, any relation between the pressures is valid if it is independent of both static and dynamic pressures, and the denominator is not zero in that zone.

Perhaps the simplest solution to the problem of the singularities might consist in applying the traditional calibration for the angular range between $\pm 30^\circ$ and then defining a different one for the remaining angles. However, as the flow angle is precisely the variable to be obtained, the problem is that it cannot be employed to discriminate the different zones. Formally, the criterion must be established through relations among the measured pressures in the holes: P_1, P_2 and P_3. Under this condition, a maximum number of six angular zones can be distinguished through the whole angular range.

Figure 3 shows the pressure distribution in the three holes of a cylindrical probe versus the flow angle. They are adimensionalized as pressure coefficients. The values in the central hole, f_1, have been adopted from the experimental measurements around a cylinder for a Reynolds number of 2.3×10^4 (taken from [24]). The distributions in the lateral holes, f_2 and f_3, have been obtained with a 45° shift of f_1. This is equivalent to an ideal cylindrical probe with real pressure coefficients. In the figure, the six main zones are highlighted: a first one when $P_1 > P_2 > P_3$ (A); a second one when $P_1 > P_3 > P_2$ (B); a third when $P_2 > P_1 > P_3$ (C); and so on. Outside

the range of $\pm 100^\circ$, no different regions to those defined within the six previous zones can be identified. Moreover, two (or even three) of the pressure sensors are measuring similar fully-detached conditions there, so this implies a physical limit of the angle determination.

In each of the six main zones, a different mathematical relation between the equations of the system (2) can be developed. Maybe, the simplest and more elegant expression is the following:

$$F(\alpha) \equiv \frac{P_j - P_k}{P_i - P_k}, \qquad P_i > P_j > P_k. \tag{4}$$

However, its application requires a previous sorting of the pressures, so its numerical implementation could be quite complex.

From a practical point of view, the best solution would be to find a unique relation covering the whole angular range, but as shown later, this is unfeasible. Therefore, it is interesting to know the minimum number zones and their associated pressure relations that could be used. To do so, a general relation with all the possible pressure combinations is introduced below.

Since any relation between the pressure values could be valid if it shows no dependence on both static and dynamic pressures, the most general relation satisfying these conditions is

$$\frac{a_1 P_1 + a_2 P_2 + a_3 P_3}{b_1 P_1 + b_2 P_2 + b_3 P_3} = \frac{a_1 f_1 + a_2 f_2 + a_3 f_3}{b_1 f_1 + b_2 f_2 + b_3 f_3} \equiv F(\alpha) \tag{5}$$

with

$$\begin{aligned} a_1 + a_2 + a_3 &= 0 \\ b_1 + b_2 + b_3 &= 0 \end{aligned} \tag{6}$$

which are the necessary restrictions to make $F(\alpha)$ independent of the static pressure. In addition, the linear combinations of coefficients a_i and b_i cannot be proportional to each other. The restrictions defined in (6) imply a reduction in the number of independent coefficients in (5) from six to four. Since the relation is conserved when multiplied or divided by any product of coefficients $a_i b_j$, this means that only two independent coefficients (one in the numerator and the other in the denominator) are really representative in $F(\alpha)$. Anyway, (5) is maintained in its more general expression, so the possibility for the coefficients a_i or b_i to be zero is not restricted.

To cover the whole angular range of possibilities—of the denominator, for example—the study could be done in three steps: first, maintaining $b_1 = 1$ and varying b_2 from 0 to -1 and b_3 from -1 to 0; second, maintaining $b_2 = 1$ and varying b_3 from 0 to -1 and b_1 from -1 to 0; and third, maintaining $b_3 = 1$ and varying b_1 from 0 to -1 and b_2 from -1 to 0. To facilitate this analysis a parameter λ has been found including the three steps. If the coefficients in the denominator (for example, again) are replaced by

$$\begin{aligned} b_1 &= \cos\left(\frac{\pi}{2}\lambda\right) \\ b_2 &= \cos\left(\frac{\pi}{2}\lambda - 120^\circ\right) \\ b_3 &= \cos\left(\frac{\pi}{2}\lambda + 120^\circ\right), \end{aligned} \tag{7}$$

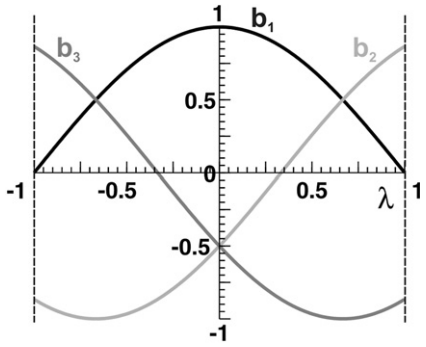

Figure 4. Coefficients b_i as a function of the λ parameter.

the variation of the λ parameter between -1 and $+1$ covers all the possible linear combinations in the denominator in (5). The previous parameter has not been mathematically deduced, it is only one of the possibilities to represent the three coefficients as a continuous function of a single variable without adding any restrictions. Figure 4 shows the coefficients (7) as a function of the λ parameter.

For example, a value of $\lambda = 0$ gives $b_1 = 1$, $b_2 = -0.5$ and $b_3 = -0.5$, i.e., the linear combination $P_1 - 0.5(P_2 + P_3)$, which is the denominator of the angular coefficient of the traditional calibration. Or applying the same equations (7) to the α_i coefficients, a value of $\lambda = 1$ gives $P_2 - P_3$, which is the numerator of the same angular coefficient.

We are going to use the λ parameter to analyse the appearance of singular points in the relation (5) (angular coefficient). Singular points arise when the denominator is zero, so

$$b_1 f_1 + b_2 f_2 + b_3 f_3 = 0. \tag{8}$$

Introducing the restriction in (6), this can be written as follows:

$$\frac{b_2}{b_1} = \frac{f_3 - f_1}{f_2 - f_3}. \tag{9}$$

Considering the b_i coefficients according to the form defined in (7), a final expression is given as a function of the λ parameter:

$$\tan\left(\frac{\pi}{2}\lambda\right) = \frac{\sqrt{3}}{3}\frac{2f_1 - f_2 - f_3}{f_2 - f_3}. \tag{10}$$

For each value of λ from -1 to $+1$ (thus covering all the possible linear combinations) one or more α values (the pressure distributions f_i are functions of α) satisfying equation (10) could be found. They correspond to the flow angles where equation (5) becomes undefined for that specific linear combination. These flow angles are plotted in figure 5 for a cylindrical probe with a construction angle of 45°. The horizontal gray lines separates the zones defined in figure 3. Note that any vertical line that could be considered in the plot intersects at least in one point with the distribution of singular points. In other words, whatever the λ parameter is, the whole angular range cannot be covered with a unique relation of the pressure values. However, if we would like to keep just one pressure relation with symmetrical features with respect to a zero-incidence angle for the attainable angular range, the only possible election for the denominator of (5) corresponds to setting $\lambda = 0$ (the denominator of the angular coefficient of

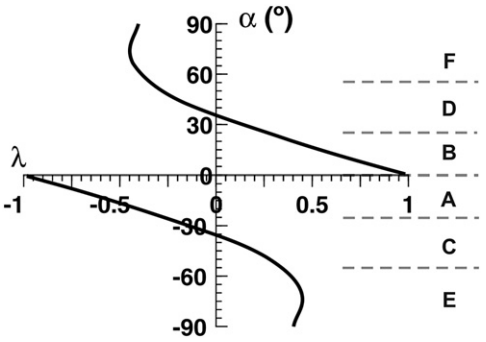

Figure 5. Distribution of singular points as a function of the λ parameter for a cylindrical probe with $\delta = 45^\circ$.

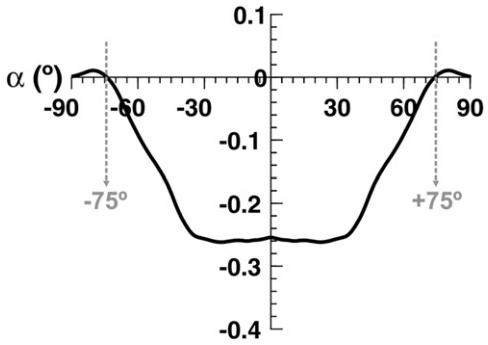

Figure 6. Double points as function of flow angle α for a cylindrical probe with $\delta = 45^\circ$.

the traditional calibration), with two singular points in $\pm 37^\circ$. Now, if we want to increase the angular range, we have to take into account more than just one zone. Thus, in order to discriminate the whole angular range with two zones, it is possible to chose any λ parameter ranging from -1 to -0.45 in the zone where $P_3 > P_2$ (B + D + F, second quadrant in figure 5) and ranging from 0.45 to 1 in the zone where $P_2 > P_3$ (A + C + E, forth quadrant in figure 5). With this double election, the whole angular range is covered with no singular points arising in the equations. For instance, adopting $\lambda = \pm 2/3$, expression (5) in the $P_3 > P_2$ zone takes the value

$$\frac{P_2 - P_3}{-P_2 + \frac{1}{2}(P_1 + P_3)} \tag{11}$$

whereas in the $P_2 > P_3$ zone is

$$\frac{P_2 - P_3}{-P_3 + \frac{1}{2}(P_1 + P_2)}. \tag{12}$$

For the numerator of all these expressions, any value of the λ parameter is valid, as long as it differs from the one chosen for the denominator. Particularly, the value $\lambda = 1$ has been fixed for the numerator in this case (in fact, a_i coefficients are defined factoring them by $2/\sqrt{3}$, which is equivalent to take $\alpha_2 = 1$ and $\alpha_3 = -1$).

2.3. Double points

Even if the problem of singularities is solved, it might be that the flow angle could not be determined univocally due to the existence of double points in the equations. This occurs when (5) becomes in a non-monotonous curve. The transition from a monotonous to a non-monotonous zone of the $F(\alpha)$ function can be identified through zeros of the flow angle derivative. Deriving $F(\alpha)$ from the general form (5)

$$\frac{\mathrm{d}F(\alpha)}{\mathrm{d}\alpha} = 0$$

$$\Rightarrow \frac{(a_1 b_2 - a_2 b_1)[(f_2 - f_3) f_1' + (f_3 - f_1) f_2' + (f_1 - f_2) f_3']}{[a_2(f_1 - f_3) + b_2(f_2 - f_3)]^2} = 0 \tag{13}$$

where f_i' represents the derivative of the pressure coefficient with respect to the flow angle, it is then deduced that the derivative turns to zero if one (or both) of the following conditions is satisfied:

$$a_1 b_2 - b_1 a_2 = 0 \tag{14}$$

$$(f_2 - f_3) f_1' + (f_3 - f_1) f_2' + (f_1 - f_2) f_3' = 0. \tag{15}$$

Note that (14) is only fulfilled if both α_i and b_i coefficients are proportional. However, this possibility was already denied when discussing the expression (5). Therefore, the only real condition that determines the presence of double points in the equations is (15). Figure 6 represents the LHS of this condition as a function of the flow angle for a cylindrical probe with an angle of 45° between the holes. The derivative presents two zeros at -75° and 75° (it is symmetrical with respect to the zero-incidence flow angle). This means that $F(\alpha)$ is monotonous for the angular interval ranging from -75° to 75°. It is important to notice that (15) is not including either α_i or b_i coefficients. As a result, any adopted expressions for $F(\alpha)$ presents double points in exactly the same angular positions. Then, the range of $\pm 75^\circ$ constitutes the maximum attainable angular range for this THP probe.

2.4. Influence of the probe construction angle

Previous analysis was conducted for a particular probe with a construction angle of 45°. Nonetheless, the angular distance between the holes might be an important parameter modifying the attainable angular range. Following, the mathematical analysis is extended to include its influence on the distribution of singularities and double points.

Figure 7 reproduces the same results shown in figure 6, but now in the case of cylindrical probes with different construction angles. Analogous considerations to those introduced in figure 3 have been assumed to set the pressure distributions for each probe. It is observed that the maximum angular range, in terms of double points restrictions, decreases with the construction angle. Note that in the case of a 65° probe, this angular range is nearly $\pm 70^\circ$, whereas for a 25° probe it could be extended even further than $\pm 90^\circ$.

To complete the analysis, the influence of the construction angle on the zones limits must also be carried out. The border limits of the six discriminating zones have been found for the construction angles from nearly 0° to 90° and plotted in figure 8 (black lines). Only positive α are represented in the figure, the negative values have a symmetrical behaviour. This

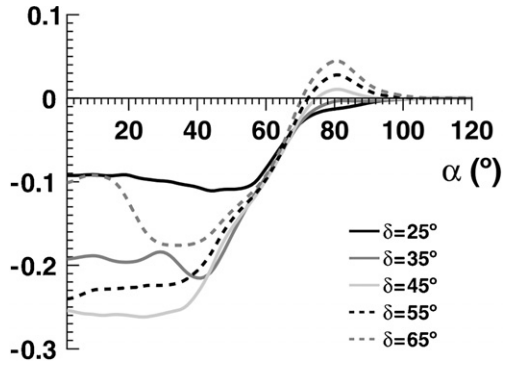

Figure 7. Location of double points for different construction angles of a cylindrical THP probe (the plot is symmetrical respect to the vertical axis).

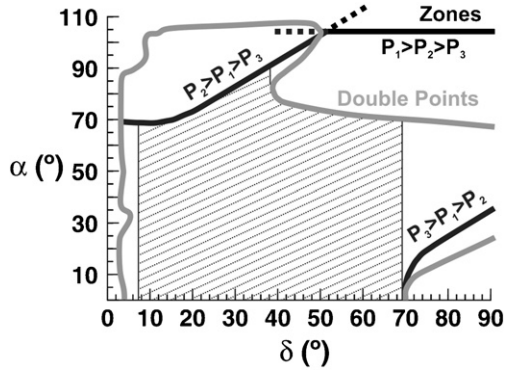

Figure 8. Limits of validity (zones and double points) as a function of δ and α for a cylindrical THP probe.

has been done for each δ using an equivalent analysis to that shown in figure 3 for $\delta = 45°$. The order in the zones changes with the construction angle; up to $\delta = 50°$ the outermost zone corresponds to $P_2 > P_1 > P_3$, while from 50° to 70° corresponds to $P_1 > P_2 > P_3$. For construction angles greater than 70° some of the zones duplicates near $\alpha = 0$ deg (line marked $P_3 > P_1 > P_2$), making this value the highest practical construction angle. Also, the flow angles where double points arise have been determined for each δ. They are also plotted in figure 8 with grey lines (cf figures 6 and 7). The shadow region in the figure shows the validity limits including both constraints. From $\delta = 7°$ to $\delta = 40°$, the maximum angular range is restricted by the discriminating zones, while from 40° to 70° the boundary is imposed by the double points. From 70° on there are also double points near $\alpha = 0°$. From the results shown in figure 8, it is possible to obtain operative ranges about ±70° for any valid construction angle. Even, theoretically, it could be possible to achieve near ±90° with a $\delta = 35°$, though no further investigations have been realized to contrast this feature.

Now, considering the methodology employed for data reduction, figure 9 shows the angular distribution of singular points, as a function of the λ parameter chosen for the denominator of the angular relation, for different construction angles of the cylindrical probe. Some differences are noticeable, especially when comparing probes with construction angles lower and higher than 45°. In particular,

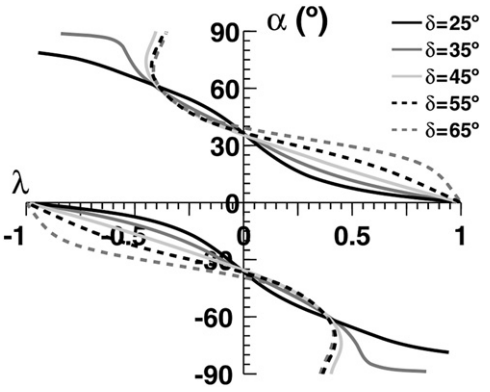

Figure 9. Singular points for different construction angles in the case of a cylindrical THP probe.

angular distances below 45° exhibit two different singular points for any relation of linear combinations (i.e., for every value of the λ parameter), so it could be necessary to introduce more than two zones to obtain the maximum angular range of the probe. Note that the traditional calibration coefficient ($\lambda = 0$) maintains the singular points in ±37°, independently of the construction angle δ. This is the reason because no angular range extension had been achieved with construction angles greater than 45°.

2.5. Dynamic and static pressure determination

In previous sections, the determination of the flow angle from the equation system (2) was discussed in detail. Once the flow angle is known, both dynamic and static pressures are obtained immediately. For instance, in the case of a particular measurement in the holes, P_1^*, P_2^*, P_3^*, that calculates the flow angle as α^*, the dynamic pressure can be obtained directly substituting these values in (5), yielding

$$P_d^* = \frac{b_1 P_1^* + b_2 P_2^* + b_3 P_3^*}{b_1 f_1(\alpha^*) + b_2 f_2(\alpha^*) + b_3 f_3(\alpha^*)}. \tag{16}$$

Finally, the static pressure is determined using any of the three equations of the system introduced in (2), for example

$$P_s^* = P_1^* - P_d^* f_1(\alpha^*). \tag{17}$$

3. Uncertainty analysis

The influence of the calibration and data reduction procedure in the uncertainty of the results is analysed in this section. For convenience, the analysis is carried out for a cylindrical probe, though it can be easily extended to include probes with other geometries. It will be shown that the uncertainty of the results is independent of the mathematical procedure that is employed for the data reduction. In addition, the influence of the construction angle of the probe in the uncertainty levels is examined carefully, in order to state which is the optimal angular distance between the holes ensuring minimal uncertainties.

3.1. Uncertainty of the flow angle and the dynamic and static pressures

The transmission of the uncertainty of the sensed pressures towards the flow angle is calculated for the generic relation of pressures combinations (5), following the method proposed by Kline [25]. Since the flow angle is determined from the pressure values P_1, P_2 and P_3, the uncertainty of the flow angle is estimated from the uncertainty of the pressure measurements according to

$$I_\alpha^2 = \left(\frac{\partial\alpha}{\partial P_1}\right)^2 I_{P_1}^2 + \left(\frac{\partial\alpha}{\partial P_2}\right)^2 I_{P_2}^2 + \left(\frac{\partial\alpha}{\partial P_3}\right)^2 I_{P_3}^2. \qquad (18)$$

Usually it is assumed that the uncertainty of the pressure measured by the transducers is the same for the three holes: $I_{P1} = I_{P2} = I_{P3} = I_P$. In (5), it was established that F is a function of the flow angle that must be determined from the calibration of the probe. Unfortunately, the flow angle is thus expressed implicitly in a discrete form, so it cannot be resolved directly through an explicit analytical solution. As a consequence, the partial derivatives of the flow angle with respect to the pressure values should be obtained using the chain rule as follows:

$$\frac{\partial\alpha}{\partial P_i} = \frac{\mathrm{d}\alpha}{\mathrm{d}F}\cdot\frac{\partial F}{\partial P_i} \qquad i = 1, 2, 3. \qquad (19)$$

However, these considerations can be reformulated in a more rigorous, mathematical form, in order to derive an expression for the uncertainty of the flow angle from the original equation system (2) without including any specific resolution method. To calculate the partial derivatives of the flow angle with respect to the pressure values measured by the probe, we differentiate the equation system (2), expressing the result in a matrix form,

$$\begin{pmatrix}\mathrm{d}P_1\\ \mathrm{d}P_2\\ \mathrm{d}P_3\end{pmatrix} = \begin{pmatrix}\partial P_1/\partial P_s & \partial P_1/\partial P_d & \partial P_1/\partial\alpha\\ \partial P_2/\partial P_s & \partial P_2/\partial P_d & \partial P_2/\partial\alpha\\ \partial P_3/\partial P_s & \partial P_3/\partial P_d & \partial P_3/\partial\alpha\end{pmatrix}\cdot\begin{pmatrix}\mathrm{d}P_s\\ \mathrm{d}P_d\\ \mathrm{d}\alpha\end{pmatrix}, \qquad (20)$$

and the derivatives are obtained inverting the Jacobian matrix in (20):

$$\frac{\partial\alpha}{\partial P_1} = \frac{f_3 - f_2}{P_d[f_1'(f_3 - f_2) + f_2'(f_1 - f_3) + f_3'(f_2 - f_1)]} \qquad (21)$$

$$\frac{\partial\alpha}{\partial P_2} = \frac{f_3 - f_1}{P_d[f_1'(f_3 - f_2) + f_2'(f_1 - f_3) + f_3'(f_2 - f_1)]} \qquad (22)$$

$$\frac{\partial\alpha}{\partial P_3} = \frac{f_2 - f_1}{P_d[f_1'(f_3 - f_2) + f_2'(f_1 - f_3) + f_3'(f_2 - f_1)]}. \qquad (23)$$

Substituting (21)–(23) into equation (18), the uncertainty of the flow angle is given by

$$I_\alpha = \frac{I_p}{P_d}\cdot\frac{\sqrt{(f_3 - f_2)^2 + (f_1 - f_3)^2 + (f_2 - f_1)^2}}{f_1'(f_3 - f_2) + f_2'(f_1 - f_3) + f_3'(f_2 - f_1)}. \qquad (24)$$

The same procedure is applied for the uncertainty levels of both dynamic and static pressures, resulting in

$$I_{P_d} = I_p\cdot\frac{\sqrt{(f_3' - f_2')^2 + (f_1' - f_3')^2 + (f_2' - f_1')^2}}{f_1'(f_3 - f_2) + f_2'(f_1 - f_3) + f_3'(f_2 - f_1)} \qquad (25)$$

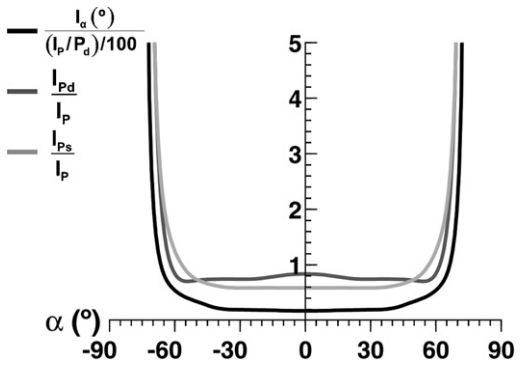

Figure 10. Distribution of the uncertainty of the flow angle and the dynamic and static pressures, over the whole angular range. A cylindrical probe with $\delta = 45^\circ$.

$$I_{P_s} = I_p\cdot\frac{\sqrt{(f_2 f_3' - f_3 f_2')^2 + (f_3 f_1' - f_1 f_3')^2 + (f_1 f_2' - f_2 f_1')^2}}{f_1'(f_3 - f_2) + f_2'(f_1 - f_3) + f_3'(f_2 - f_1)}. \qquad (26)$$

The uncertainties are different for every specific probe, but they are independent of any data reduction procedure, if the procedure is an exact mathematical method. Let consider a particular measurement with real pressure values denoted as P_1^*, P_2^*, P_3^*, corresponding to a real flow angle α^*. Suppose that an error is introduced when measuring one of these pressure values, for instance, obtaining P_1^{**} instead of P_1^*. If the data reduction technique is an exact solution of the equation system (2), the resulting flow angle will be always the same, α^{**}, whatever procedure is employed. In other words, an uncertainty of the measurements, $I_{P_1} = |P_1^* - P_1^{**}|$, leads to an uncertainty in the flow angle, $I_\alpha = |\alpha^* - \alpha^{**}|$, which is independent of the resolution method. Moreover, this has also been proved using the general form of $F(\alpha)$ in equation (5) to obtain the partial derivatives in equation (19). Although the mathematical development is not detailed here for brevity, both α_i and b_i coefficients cancel out and the same expressions, previously formulated in (21)–(23), are obtained.

Figure 10 shows the uncertainties over the whole range of a cylindrical probe with a construction angle of 45°. The uncertainty of the flow angle is expressed as a percentage of the uncertainty in the pressure measurement, I_P, relative to the dynamic pressure P_d, while both dynamic and static pressures uncertainties are only referred to I_P, as befit the equations. When $\alpha = 0^\circ$, the uncertainty in the flow angle is about 0.15° for every 1% of I_P/P_d. This uncertainty level is maintained for all the angles ranged between ±30°. Outside this range, the levels increase progressively, reaching up to 0.5 when $\alpha = \pm 60^\circ$. The uncertainty rises severely when operating in the limits of the attainable angular range of these probes ($\alpha = \pm 70^\circ$). The uncertainty of the dynamic and static pressures follow, basically, the same behaviour than the flow angle. They are practically constant for a wide region of the angular range (close to ±60°), with characteristic values lower than unity.

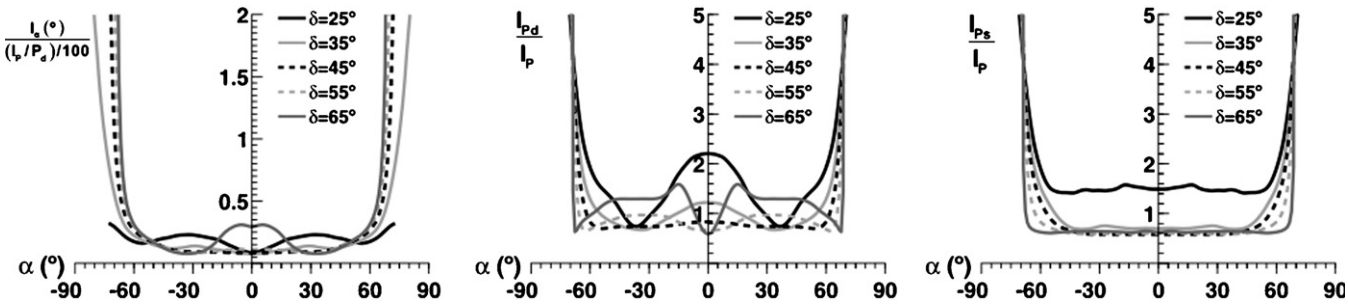

Figure 11. Influence of the probe construction angle in the uncertainty levels of the flow angle and both dynamic and static pressures for a cylindrical probe.

3.2. Effects of the construction angle

Construction angles going from 10° to 70° have been considered to analyse the effects of the angular distance between the holes on the uncertainty levels. Such an interval has been selected according to the limits of δ angles shown in figure 8. Figure 11 shows the uncertainty results for the flow angle and both dynamic and static pressure with five of the different construction angles studied. In general, the angle uncertainty presents reasonable low levels for all the construction angles, without exceeding 0.35° for every 1% of I_P/P_d. For intermediate values of the construction angle, the angle uncertainty is quite uniform for central values of α. This uniformity is lost for extreme angular distances of the holes ($\delta \leqslant 25$ or $\delta \geqslant 65°$). In particular, in the case of $\delta \leqslant 25°$, a sudden increase of I_α appears for flow angles around ±30°, whereas maximum uncertainties are concentrated close to zero-incidence flows when $\delta \geqslant 65°$.

Distributions for the uncertainty of the dynamic pressure are more uniform if the construction angle lies between 40° and 60°. When the angular distance of the holes is 25° (or lower), a significant increase of I_{Pd} appears around $\alpha = 0°$, whereas in the case of $\delta \geqslant 65°$, lowest values of I_{Pd} are encountered for zero-incidence flows.

Complementarily, the uncertainty of the static pressure is quite uniform for all the construction angles. Nevertheless, a considerable increment of I_{Ps} is observed all over the angular range of the probe when $\delta \leqslant 25°$.

As a conclusion, bearing in mind the results shown in figures 8 and 11, the more desirable design of cylindrical probes is achieved when the angular distance between the holes ranges from 30° to 60°. Within this interval, the uncertainty is reasonable low and very similar for all the situations. Even cylindrical THP probes with construction angles between 60° and 70° can be employed; uncertainty values are larger but still acceptable. In contrast, construction angles lower than 30° are not recommended, due to the notable increase of the uncertainty levels for both dynamic and static pressures.

4. Measurement test

In this section, the methodology developed above is illustrated with calibrations and measurements using real probes. They have been mostly conducted with pneumatic probes in uniform steady flow, but also an example of a dynamic measurement in a turbomachine is included.

4.1. Calibration

The test rig is a small wind tunnel, composed of a centrifugal fan at the inlet, a settling chamber and a 4:1 contraction nozzle that ensures uniform flow. It has an opened working area of 0.15 × 0.30 m^2 where the probe is operated (the static pressure is thus atmospheric). The maximum attainable velocity is 65 m s^{-1}, with a turbulence level around 0.5%. The velocity magnitude is determined with a Pitot-static probe at the measurement section (and with the pressure in the settling chamber). These pressures are measured with U-manometers and pressure transducers. The uncertainty for the mean velocity is estimated to be lower than 0.2%. The probes are held in a rotating support, driven by a step motor, so they can be axially rotated 360° with a precision higher than 0.1°.

The probes tested are cylindrical three-hole probes with construction angles of 30°, 45° and 60°. Here, most of the results given here correspond to the 45° probe. The diameter of the probes is 8 mm, with variable shaft lengths. The head is about 24 mm and the three-holes arrangement is placed 16 mm from the semi-spherical tip, with a 0.8 mm hole diameter. In addition, the internal tubing of the probe has a 1 mm inner diameter, and 0.5 m length. Two meters of pneumatic tube, 4 mm internal diameter, are used to connect the internal tubes with each transducer. The transducers are Validyne DP15, with a 350 mm H_2O range and accuracy of ±0.25%. Its amplified output was acquired with a PCI 12bits A/D card.

Measurements were taken adjusting the velocity in the test section and positioning the probe at the desired angles. A sampling frequency of 1 kHz per channel was found to be accurate enough due to the low frequency response of the instrumentation assembly. The samples, stored as raw data, are numerically post-processed to obtain the mean values. Several filters can be used in the electronic hardware and also in the digital processing of the signals, to avoid aliasing and to filter the desired frequencies out.

From the different possibilities that can be used in the data reduction procedure, a two-zone method has been chosen, with the following relations:

$$\frac{P_2 - P_3}{P_1 + P_2 - 2P_3} = \frac{f_2 - f_3}{f_1 + f_2 - 2f_3} = F(\alpha) \quad \text{when } P_2 > P_3 \tag{27}$$

and

$$\frac{P_2 - P_3}{P_1 + P_3 - 2P_2} = \frac{f_2 - f_3}{f_1 + f_3 - 2f_2} = F(\alpha) \quad \text{when } P_3 > P_2. \tag{28}$$

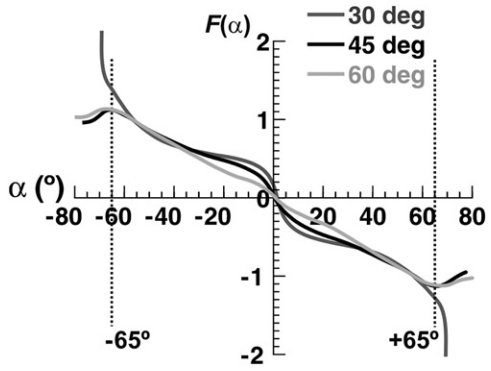

Figure 12. Angular coefficients, $F(\alpha)$, of three cylindrical probes with 30°, 45° and 60° construction angles ($Re = 2 \times 10^4$).

This definition is equivalent to a parameter $\lambda = \pm 2/3$ in the denominator of equation (5) and $\lambda = -1$ in the numerator.

The three pneumatic probes mentioned above have been calibrated with a velocity of 36.4 m s^{-1} ($Re = 2 \times 10^4$), covering the flow angles (angular positions of the probe, really) between −90° and +90° with a 5° interval. With the pressures acquired during calibration, both traditional and zone-based angular coefficients are obtained.

Coefficients defined though (27)–(28) are plotted in figure 12 for the three construction angles. The 30° configuration presents two singular points near the ±70° flow angle. Both 45° and 60° probes have two double point limits about ±65°. It is suspected that these probes do not reach the ±70° angular span due to three-dimensional effects induced by the proximity of the probe tip and the specific adopted Reynolds. The traditional calibration is also restricted to ±30°.

According to figure 8, it is possible that the 30° probe may provide an operative angular range about ±85°; however, in order to avoid the singularities, a three-zone data reduction technique would be necessary.

The pressure coefficients and the measurements standard deviation taken from the 45° probe calibration are shown in figure 13. The standard deviation is an uncertainty indicator of a single sample in the measurements. It includes the transducers and measurement system accuracy, the test rig uncertainty and the aerodynamic characteristics of the probe for this particular assembly (systematic errors are not considered). The standard deviation increases with the flow angle relative to each hole, going approximately from 0.7% when the hole is facing the flow to 1.2% when the hole is in the separated region. Although a progressive increment is observed, no abrupt change is found when the separation is set off.

This probe geometry has a vortex-shedding phenomenon with a Strouhal number around 0.2. However, the frequency response of the probe assembly is much lower, and the increment in the standard deviation seems to be more related to the pressure coefficient value rather than to any unsteady phenomena. At least, with this particular probe and setup, there are no significant differences between the ±35° and the ±70° ranges. Obviously, this cannot be the same for fast response probes.

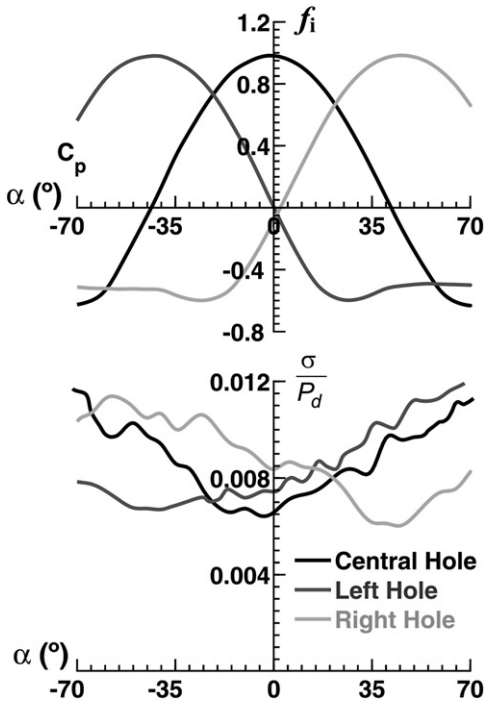

Figure 13. Pressure coefficients and standard deviation of calibration measurements with a 45° probe ($Re = 2 \times 10^4$).

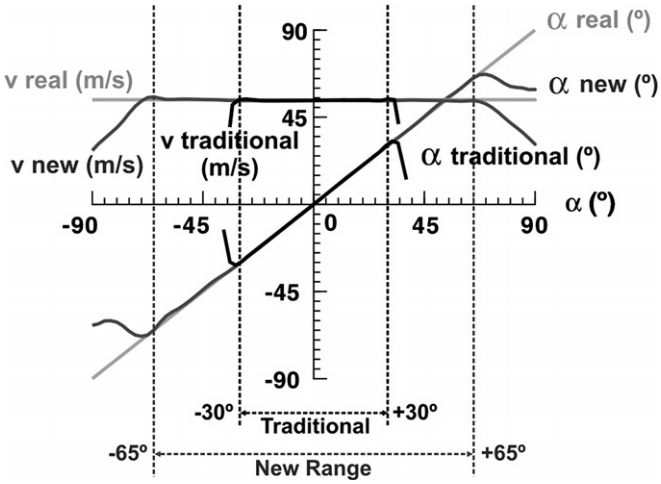

Figure 14. Comparison between the traditional and new reduction method with measurements between ±90° with a $Re = 3 \times 10^4$.

4.2. Data reduction comparison and the Reynolds number effect

To compare the results obtained using the traditional calibration and the new data reduction procedure, a set of measurements have been conducted for a velocity of 54 m s^{-1} ($Re = 3 \times 10^4$) with flow angles varying between ±90° every 2.5°. The acquisition settings were maintained from previous measurements. Figure 14 shows the results obtained with each technique, compared to the real values of the flow. Inside the traditional calibration range, both methods give the same solutions, but with the new procedure, an extended angular span is covered. Outside the valid ranges of each calibration method, the results usually provide a wrong flow angle (staying

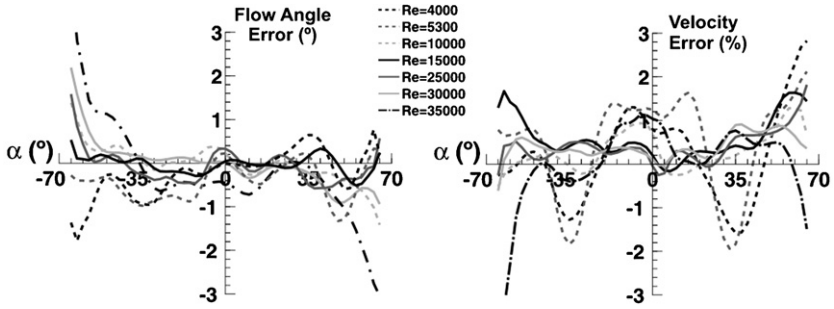

Figure 15. Reynolds influence on the flow angle and velocity errors for a 45° cylindrical probe using a $Re = 2 \times 10^4$ calibration.

inside the limits of the angular span). The sharp changes in the range boundary of the traditional calibration are due to the mathematical singularities.

To define the influence of the Reynolds number in the probe calibration, several measurements were acquired from $Re = 4 \times 10^3$ to $Re = 3.5 \times 10^4$. They have been transformed using the calibration corresponding to $Re = 2 \times 10^4$. Since the real probe angle and the velocity magnitude of the flow in the test rig are known for each measurement, it is possible to calculate the error (figure 15). For most of the angular span, the difference in the flow angle lies between $\pm 1^\circ$ and between $\pm 2\%$ in the velocity magnitude. Lower Reynolds numbers show significant errors, not only in the extended range but also in the traditional one (especially for the velocity magnitude). For the highest Reynolds number (3.5×10^4), the errors in both angle and velocity values increase suddenly close to the borders of the angular range. Also, noticeable differences in the velocity magnitude are found in the central zone. Complementarily, the standard deviation increases as the Reynolds number decreases (not shown here). Values for $Re = 4 \times 10^3$ are as high as 5% of P_d, maintaining similar trends to those previously reported in figure 13.

In essence, the analysis of the previous tests shows that with pneumatic probes for stationary flows, the new data reduction method attains the same performance as the traditional one, providing a wider angular range.

4.3. Dynamic measurements with a fast response probe

Additional measurements, now with a dynamic probe, are reported below. Since only averaged values are compared with hot wire measurements, this section constitutes an application example rather than a validation. This dynamic probe, with a geometry similar to the pneumatic one, has three miniature pressure sensors placed axially inside the probe, at 6 mm from the holes openings. The construction angle is 60° (it was built during the initial stages of the investigation). The Kulite CCQ-093 pressure sensors have 2.4 mm diameter and 9.5 mm length, with a differential pressure range of 0.35 bar, accuracy of $\pm 0.1\%$ and a natural frequency of 150 kHz.

The probe has been calibrated in the same facility as the pneumatic probes. The vortex shedding phenomena has been overcome with a higher sampling frequency (2 kHz), larger acquiring sequences (up to 5000 points) and an averaging process for every angular position. In this case, a remarkable

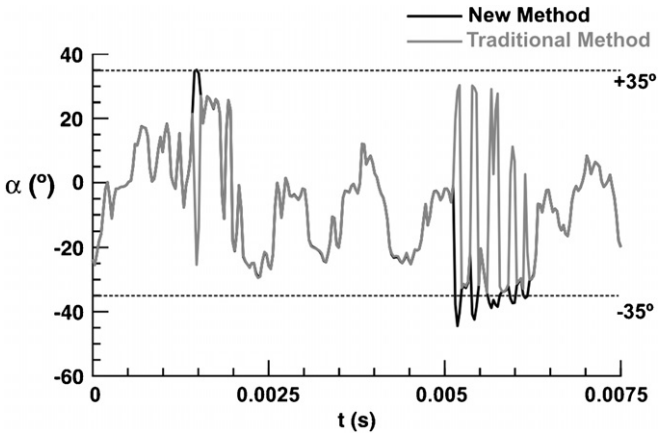

Figure 16. Instantaneous flow angle in a low-speed axial fan. Comparison between data reduction methods.

increase is found in the standard deviation when a hole is in the separated flow region. However, the mean values of the pressure coefficient were found to be very close to those obtained with the pneumatic probe.

Some measurements have been conducted with the dynamic probe in a low-speed axial fan with inlet guide vanes. This stator-rotor configuration is composed of 13 fixed vanes and a 9-blade rotor running at 2400 rpm, with hub and tip diameters of 380 and 820 mm, respectively (more details can be found in [26]). The probe, placed 30 mm downstream of the rotor blades, was employed to obtain several spanwise measurements, with an acquisition frequency of 36 kHz and 10 000 samples per channel (the blade passing frequency BPF is 360 Hz).

Figure 16 shows the flow angle from an instantaneous measurement in the hub region (10% span), transformed with both traditional and new data reduction methods. These extreme angular oscillations are only observed near the hub and the tip regions. The flow angle in the central part of the span usually stays inside the traditional range. The instantaneous signals were ensemble-averaged to obtain the blade-to-blade distributions, as shown in figure 17(*a*). Measurements near the hub (10% span), tip (90% span) and midspan are compared with the equivalent measurements taken with dual hot wire anemometry (DHW). Figure 17(*b*) shows the power spectra of the instantaneous measurement at midspan for the central and one lateral hole of the probe.

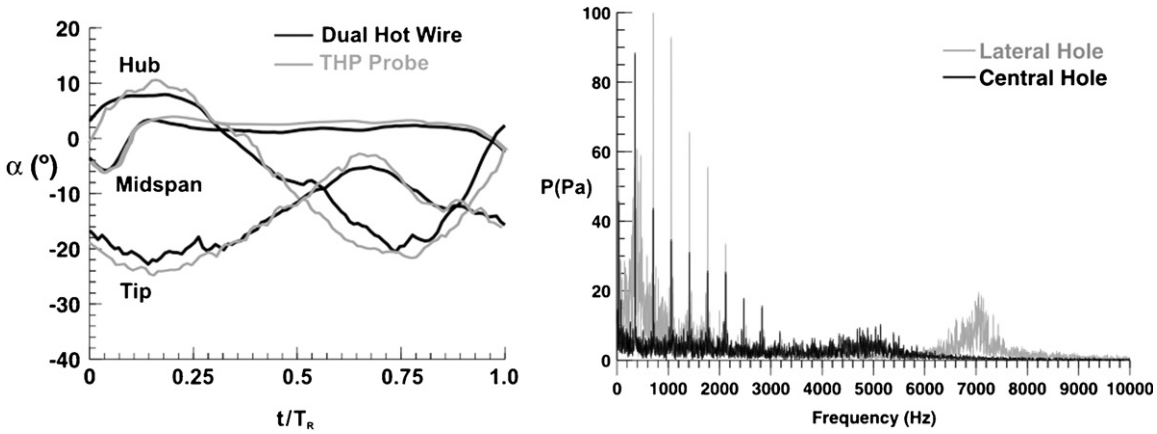

Figure 17. (*a*) Ensemble-averaged distributions in a low-speed axial fan (comparison with DHW data); (*b*) power spectra of the instantaneous signal at midspan. $T_R = 1/\text{BPF}$.

The midspan measurement exhibits an unsteadiness about 5 kHz for the central hole and 7 kHz for the lateral hole, clearly seen in figure 17(*b*). This is linked to the frequency response of the line-cavity system connecting the pressure tap with the sensor (a one-dimensional analytical estimation [27] shows a resonance frequency around 6 kHz and 9 kHz, respectively). In this application, this phenomenon can be filtered without significant information loss. In contrast, the increment in the noise level registered at low frequencies in the lateral holes is not so easy to eliminate, although it can be notably segregated by means of the ensemble-averaging operator. This noise has been related to the lateral holes measurements in the separated flow region, it does not seem directly linked to the probe vortex-shedding frequency (1100 Hz at midspan). The high unsteadiness of the flow near the hub and the tip makes both mentioned phenomena disappear, with the spectral content of the instantaneous pressure probe measurement being practically the same as the DHW probe (although the averaged results are noisier).

An additional consideration for fast response probes is that the extended range is partially achieved with one of the holes in the separated flow region. With slow response probes this is not generally a major inconvenient, but with fast response probes it could become a severe limitation because the lateral holes measuring in the separated flow region usually present unsuitable performances. As the separation begins around 82°, for a probe built with a construction angle of 45° the maximum angular range avoiding the separated flow region is limited to ±37°, and it can be covered with the traditional calibration. With smaller construction angles, wider separated-free angular ranges can be achieved, although if it is smaller than 25°, the uncertainty transmission increases severely. Thus, the optimal construction angle for fast response probes is around 30°, which provides an extended range of about ±50° with no holes measuring in separated regions.

Also, though this exceeds the aim of the paper, other THP probe geometries, as trapezoidal or cobra-type probes, may have better characteristics with respect to the separation zone and take better advantage of the extended range.

5. Conclusions

A mathematical analysis of the equation system that describes the behaviour of the pressure distributions in the holes of THP probes has been carried out. The analysis, based on a theoretical cylindrical probe, has provided the conditions limiting the attainable angular range of the probes: singularities and double points in the equations of the data reduction method.

A direct procedure for data reduction has been proposed to improve the operative angular range of THP probes. For that purpose, several zones along the angular range have been discriminated, using the pressure values measured in the holes. Then, a different reducing equation is applied for each zone, ensuring that no singularities arise.

The influence of the probe construction angle over the operative angular range has also been analysed. For cylindrical probes, it has been established that, with a construction angle between 10° and 70°, it is possible to obtain operative angular ranges of about ±70° when using the proposed data reduction. This span is two times broader than the one usually achieved.

In addition, the influence of the resolution methodology on the uncertainty of the results has been studied. It was concluded that the uncertainty transmission is independent of the mathematical procedure employed for the data reduction. The effect of the construction angle on the uncertainty was also considered, pointing out that angular distances between the holes from 30° to 60° present the lowest uncertainty levels.

Using a low response cylindrical probe, the new data reduction technique has been contrasted with the traditional calibration over the same experimental data. The comparison shows that both methods obtain identical results inside the traditional angular range, but with the advantage of an extended span (from ±65° to ±80°) for the new procedure. Fast response probes should avoid measurements with a hole in the separated flow region of the probe. For cylindrical probes with construction angles higher than 45°, this restriction makes the extended angular range of the new proposal only marginally better than the traditional one. As the uncertainty substantially increases for construction angles smaller than 25°, the optimal construction angle for fast response probes is

around 30°, providing an angular range of ±50° with the new data reduction method.

Acknowledgments

This work was supported by the Research Project 'Effect of the volute geometry of centrifugal pumps on the fluid-dynamic perturbations due to rotor-stator interaction', ref. DPI-2006-15638-C02-01, MEC.

References

[1] Pope A and Harper J J 1966 *Low-Speed Wind Tunnel Testing* (New York: Wiley)
[2] Dudziniski T J and Krause L N 1969 Flow-direction measurement with fixed-position probes *NASA TM X-1904*
[3] Blanco E, Ballesteros R and Santolaria C 1998 Angular range and uncertainty analysis of non-orthogonal crossed hot wire probes *J. Fluids Eng.* **120** 90–4
[4] Dudziniski T J and Krause L N 1971 Effect of inlet geometry on flow-angle characteristics of miniature total-pressure tubes *NASA TN D-6406*
[5] Erwin J R 1964 *Experimental Techniques. Section D of Aerodynamics of Turbines and Compressors* (Princeton, NJ: Princeton University Press)
[6] Ligrani P M, Singer B A and Braum L R 1989 Miniature five-hole pressure probe for measurement of three mean velocity components in low-speed flows *J. Phys. E: Sci. Instrum.* **22** 868–76
[7] Gameiro M C, Pereira C A C and Cruz J M S 2001 On the use of a linear interpolation method in the measurement procedure of a seven-hole pressure probe *Exp. Therm. Fluid Sci.* **28** 1–8
[8] Ingram G and Gregory-Smith D 2006 An automated instrumentation system for flow and loss measurements in a cascade *Flow Meas. Instrum.* **17** 23–28
[9] Bakhtar F, Mashmoushy H and Jadayel H C 2001 Calibration characteristics of a three-hole probe and a static tube in wet steam *Int. J. Heat Fluid Flow* **22** 537–42
[10] Hooper J D and Musgrove A R 1997 Reynolds stress, mean velocity, and dynamic static pressure measurement by a four-hole pressure probe *Exp. Therm. Fluid Sci.* **15** 375–83
[11] Guo Y and Wood D H 2001 Instantaneous velocity and pressure measurements in turbulent mixing layers *Exp. Therm. Fluid Sci.* **24** 139–50
[12] Chen J, Haynes B S and Fletcher D F 2000 Cobra probe measurements of mean velocities, Reynolds stresses and higher-order velocity correlations in pipe flow *Exp. Therm. Fluid Sci.* **21** 206–17
[13] Kupferschmied P, Köppel P, Gizzi W, Roduner C and Gyarmathy G 2000 Time-resolved for measurements with fast-response aerodynamic probes in turbomachines *Meas. Sci. Technol.* **11** 1036–54
[14] Wuest W 1967 Measurement of flow speed and flow direction by aerodynamic probes and vanes *AGARD Conf. Proc.* vol 32 pp 373–426
[15] Bryer D W and Pankhurst R C 1974 *Pressure-Probe Methods for determining Wind Speed and Flow Direction* (Teddington: National Physical Laboratory) (ISBN: 011-480012X) **Q1**
[16] Lewis W E 1966 Fixed-direction probes for aerodynamic measurements *Proc. Inst. Mech. Eng.* **180** 141–52
[17] Everett K N, Gerner A A and Durston D A 1983 Seven-hole probe for high angle flow measurement: Theory and Calibration *AIAA J.* **21** 992–8
[18] Gallington R W 1978 Measurement of very Large Flow Angles with Non-Nulling Seven-Hole Probes *Aeronaut. Dig.* **Q2**
[19] Treaster A L and Yocum A M 1979 The calibration and application of five-hole probes *ISA Trans.* **18** 23–34
[20] Kjelgaard S O 1988 Theoretical derivation and calibration technique of a hemispherical-tipped five-hole probe *NASA TM 4047*
[21] Zilliac G G 1989 Calibration of seven-hole pressure probes for use in fluid flows with large angularity *NASA TM 102200*
[22] Sumner D 2002 A comparison of data-reduction methods for a seven-hole probe *J. Fluids Eng.* **124** 523–7
[23] Contini D, Manfrida G and Michelassi V 1999 Secondary flow measurements in a gas turbine cascade by a 3D pneumatic probe *14th Symp. on Measuring Techniques for Transonic and Supersonic Flows in Cascades and Turbomachines (Limerick, Ireland)*
[24] Weidman P D 1968 Wake transition and blockage effects on cylinder base pressures *PhD Thesis* California Institute of Technology
[25] Kline S J and McClintock F A 1953 Describing uncertainties in single sample experiments *Mech. Eng.* 3–8
[26] Fernández Oro J M, Argüelles Díaz K M, Santolaria Morros C and Blanco Marigorta E 2007 Unsteady flow and wake transport in a low-speed axial fan with inlet guide vanes *J. Fluids Eng.* **129** 1015–1029
[27] Persico G, Gaetani P and Guardone A 2005 Design and analysis of new concept fast-response pressure probes *Meas. Sci. Technol.* **16** 1741–50

Queries

(1) Author: Please check whether the location of the publisher in reference [15] is okay as set.
(2) Author: Please provide volume and page number in reference [18].
